Accepted Manuscript

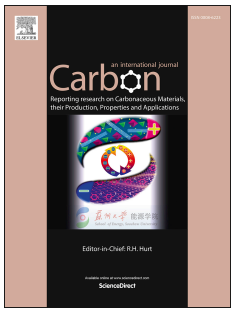

Synthesis of reduced graphene oxide (rGO) films onto carbon steel by cathodic electrophoretic deposition: Anticorrosive coating

J.A. Quezada-Rentería, L.F. Cházaro-Ruiz, J.R. Rangel-Mendez

PII: S0008-6223(17)30651-6

DOI: 10.1016/j.carbon.2017.06.074

Reference: CARBON 12138

To appear in: *Carbon*

Received Date: 17 February 2017

Revised Date: 21 June 2017

Accepted Date: 22 June 2017

Please cite this article as: J.A. Quezada-Rentería, L.F. Cházaro-Ruiz, J.R. Rangel-Mendez, Synthesis of reduced graphene oxide (rGO) films onto carbon steel by cathodic electrophoretic deposition: Anticorrosive coating, *Carbon* (2017), doi: 10.1016/j.carbon.2017.06.074.

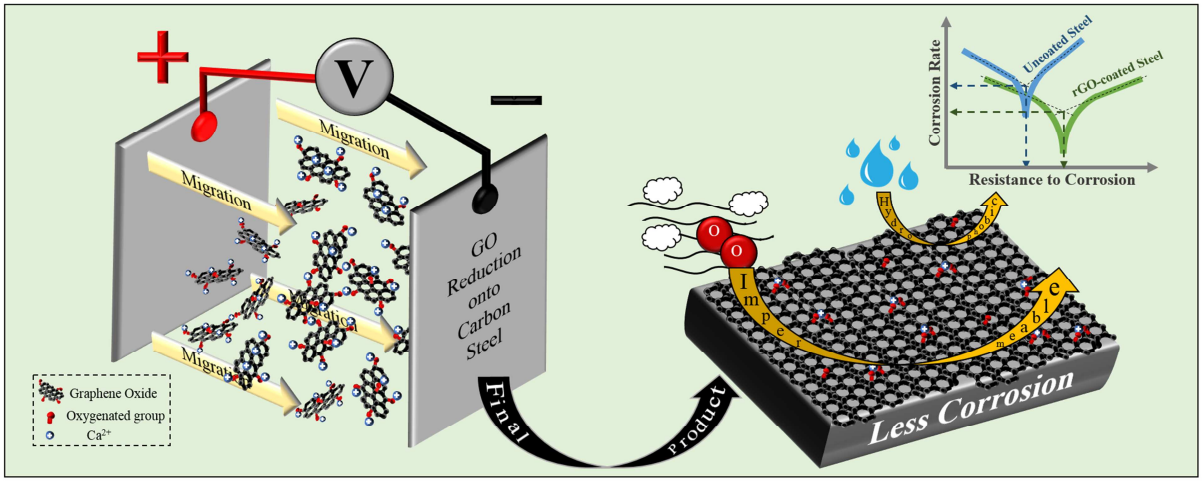

Synthesis of reduced graphene oxide (rGO) films onto carbon steel by cathodic electrophoretic deposition: anticorrosive coating

J. A. Quezada-Rentería[a], L. F. Cházaro-Ruiz[a]*, J. R. Rangel-Mendez[a]*

[a] División de Ciencias Ambientales, Instituto Potosino de Investigación Científica y Tecnológica A.C., Camino a la Presa San José 2055, Col. Lomas 4ª Sección, C.P. 78216, San Luis Potosí, SLP, México.

Abstract

The use of graphene based materials as anticorrosive coatings for the protection of metals is still a controversial subject worthy of debate. The electrophoretic deposition (EPD) is one of the most used techniques to produce anticorrosive coatings onto metals, including graphene oxide (GO) and reduced graphene oxide (rGO) coatings. However, for the specific case of carbon steel's protection, EPD of GO has not achieved positive results. This work proposes a variation in the EPD process of GO, which consisted in changing the GO's charge to positive values by adsorbing Ca^{2+}, allowing the electrophoretic deposition of GO onto the cathode (cEPD). The achieved film was characterized by scanning electron microscopy (SEM), Raman Spectroscopy, X-ray photoelectron spectroscopy (XPS) and evaluated electrochemically. The coating diminished by three times the corrosion of carbon steel: the corrosion current was reduced from 11.83 to 4.14 mA cm^{-2}, the charge transfer resistance incremented from 84 to 406 Ω and a shift in the corrosion potential from -0.72 to -0.61 V was observed. An electrochemical reduction mechanism of GO involving hydrogenation/hydrogenolysis reactions is suggested as the main reason to achieved an effective coating by cEPD in comparison to the films produced by an anodic EPD.

*Corresponding authors.
E-mail address: rene@ipicyt.edu.mx, phone number: 8342000 Ext. 2022 (J. R. Rangél-Méndez).
E-mail address: luis.chazaro@ipicyt.edu.mx, phone number: 8342000 Ext. 2041 (L. F. Cházaro-Ruiz).

Keywords: Graphene Oxide, Reduced Graphene Oxide, Electrophoretic Deposition, Anticorrosive coating, Carbon Steel

1. Introduction

Graphene is a 2D honeycomb lattice composed only of carbon atoms with sp^2 hybridization [1], this structure confers it a wide range of properties, such as, high electrical conductivity, excellent mechanical properties, impermeability, hydrophobicity and an excellent transparency (absorbing only 2.3% of the incoming light) [2–5]. These properties have interested scientists to use it in numerous applications, including its use as an anticorrosive coating for the protection of metals. For example, it has been reported that the CVD-grown graphene decreases the corrosion rate of metals, especially for Cu and Ni [6–9]. However, with this methodology, graphene can only be synthetized on a limited number of substrates, and complications arise when trying to transfer the CVD-grown graphene to another substrate in order to protect it from corrosion, since the graphene sheet tends to break during the transfer procedure, creating sites that promote the corrosion [6,10]. This problem, together with the high costs of this technique, has motivated scientist to search for more practical ways to produce graphene based films or coatings. A chemical production of graphene via graphene oxide (GO) is considered to be the most viable option for the large-scale synthesis of graphene based materials [11]. GO is an oxygen functionalized form of graphene, and the presence of this groups leads to the alteration or loss of some properties, such as its high electrical conductivity and hydrophobicity; however, the properties of pristine graphene can be restored, until a certain degree, by removing the oxygenated functionalities from GO using different methods [12]. Additionally, GO presents the

advantage of being easily dispersed in water [13], which facilitates the assembly of macrostructures, by numerous methods, among which is the electrophoretic deposition (EPD) of GO. In this method, an electric field is used to cause the migration of the GO sheets, due to the negative charge that they develop when suspended in water, to the electrode of opposite charge, which in this case is the anode, forming uniform and thickness-controlled films [14]. In addition, the formation of the deposit is accompanied by the removal of the oxygenated groups of GO via an electrochemical oxidation, where specifically the carboxylic acids are gone in the form of CO_2 [15,16], therefore, obtaining a reduced graphene oxide film (rGO). The anodic electrophoretic deposition (aEPD) of GO has been widely used to produce films for a wide range of applications, including the protection of metals from corrosion [17], giving good results for the protection of metals such as copper [18,19]. However for the specific case of carbon steel, the aEPD of GO has not given positive results, the latter is owed to the formation of defects, such as vacancies, during the anodic oxidation process [20]. This work considers the cathodic electrophoretic deposition (cEPD) of GO as an alternative to the disadvantage of aEPD, since it is believed that the electrochemical reduction mechanism is rather different from the electrochemical oxidation in GO [21]. To achieve the cEPD, the negative charge of GO has to be inverted, which can be accomplished by the use of surfactant agents, like polyelectrolytes [22], and with heavy metal ions, such as Ni, Co and Zn, in the GO suspension [23–25]. However, these approaches have as a disadvantage the production of a composite film, which, although has given positive results as an anticorrosive coating for some metals, adds nothing to the existing doubt about the capacity of graphene and rGO films to perform as barriers for protection against corrosion [26]. Additionally, the reported works where heavy metal ions are added to the suspension [23–25], utilized an excessive concentration of salts,

which affects the mass transport by migration, making necessary the use of convection as an additional mass transport mechanism, which also affects the EPD process. Hence, the approach used in this work was to use a surfactant-free suspension of GO, in which the charge of GO sheets is controlled by the chemical nature, pH and ionic strength of the suspension, to avoid migration problems and to obtain a rGO film by cEPD, which was evaluated as an anticorrosive coating for protecting carbon steel.

2. Materials and Methods

2.1 Substances and Materials

A commercial suspension of GO from the brand Graphene supermarket, which contained 6.2 g L^{-1} of GO in water, was used to prepare all the GO suspensions used in this work. Also, $CaCl_2$ salt was used in the preparation of the different electrolytic solutions, the salt was analytical grade from Fermont and it was used as received. All the solutions were made using deionized water with a resistivity of 18 MΩ cm. Either HCl or NaOH 0.1 M standard solutions from Fermont where used to adjust the pH of the solutions and GO suspensions used in this work. AISI 1045 medium carbon steel was used in this study, which has a chemical composition of 0.43-0.50 % C, 0.60-0.90 % Mn, 0.04 % P (max), and 0.05 % S (max).

2.2 GO Characterization

2.2.1 Zeta potential (ζ) and particle size measurement

Zeta potential and particle size measurements of GO sheets in aqueous suspensions were conducted by using a particle size analyzer Zetatrac Nanotrac, in a pH range from 2 to 11. The GO concentration in the suspension was 200 mg L^{-1}.

2.2.2 Boehm Titration

Boehm titration protocol was used to determine the concentration of acid groups on the GO sheets. 0.003 g of GO were contacted with bases of different pK_b ($NaHCO_3$, Na_2CO_3, NaOH and $NaOC_2H_5$), all of them in a concentration of 0.1 M. After a short period of incubation at 25 °C and 120 rpm, the suspensions where titrated with HCl 0.1 M by an automatic titrator Metler Toledo. It is important to specify that the suspensions where sparked with N_2 before the incubation time and the titration procedure, in order to remove the CO_2 from solution. The concentration of the different acid groups was estimated considering their corresponding pK_a's values, as stablished by Boehm [27].

2.2.3 FT-IR

The infrared spectrum of GO was obtained using KBr pellets as a support and background. In order to prepare the pellets, the GO sample and the KBr salt were dried at 45 and 85 °C, respectively, in a vacuum oven during 72 h. The pellets contained GO in a proportion of

0.46 % (w/w). The FT-IR scan was made in transmittance mode, with 128 scans and a resolution of 4 cm^{-1} in a wavelength range from 550 to 4000 cm^{-1}.

2.2.4 Calcium adsorption isotherms

Adsorption essays were made at 25 °C at two constant pH values, 4 and 6. To do this, 3 mg of GO were contacted with 15 mL of a $CaCl_2$ solution, in a concentration range from 0.001 to 0.175 M. The system was shaken at 120 rpm and the pH was constantly monitored and adjusted to either 4 or 6 until the equilibrium was reached. The Ca^{2+} residual concentration in solution was determined by ICP-MS.

2.3 EPD of GO

The experimental set up for the EPD of GO consisted in two parallel electrodes cell, where the carbon steel electrode was used as a cathode and a graphite plaque as anode, the electrodes were separated 10 mm. The suspension contained 200 ppm of GO, $CaCl_2$ in a concentration of 0.1 M, and the pH was adjusted to 6. The voltage applied was chosen in function of the reduction potential of GO, and the perturbation lasted 90 min. After the synthesis of the films, the coated pieces of steel were rinsed with deionized water and dried with an ethanol/acetone mixture.

2.4 EPD rGO film characterization

2.4.1 Raman

Raman spectra were obtained using a Renishaw Invia Raman Microscope, equipped with a 532 nm wavelength incident laser and a 100x objective. The spectrum of GO was obtained by drop coating a piece of carbon steel with GO, in order to compare the spectra to those obtained after the cEPD process.

2.4.2 SEM

The SEM micrographs were obtained with a FEI Qaunta FEI 250 using high vacuum. EDS was performed on the rGO-coated and uncoated steel samples using a voltage of 5 KeV.

2.4.3 XPS

XPS measurements were performed on a PHI 5000 VersaProbe II system from Physical Electronicas, employing a monochromatic Al-Kα X-ray source with 1486.6 eV energy and a charge neutralizer system. The beam size used was 100 μm with a power and voltage of 25 W and 15 KV, respectively. The survey spectra were obtained using pass energy of 117.40 eV and a 1 eV step size by doing 5 sweeps. Meanwhile, the high definition spectra were obtained using pass energy of 23.5 eV and a 0.2 eV step size and 50 sweeps.

2.5 Electrochemical analysis for the corrosion assessment

The characterization of the anticorrosive properties of the synthetized films was made through linear polarization and electrochemical impedance spectroscopy (EIS). For both cases, a three-electrode cell was employed, where a piece of carbon steel (CS), either coated or uncoated with rGO, was used as working electrode (exposed area of 0.7854 cm^2), a graphite plate was used as counter electrode and the Ag/AgCl/NaCl (3 M) system was used as reference electrode, the latter was inside a glass prolongation filled with electrolyte. NaCl 3.5 % w/v was used as electrolyte medium; the solution was sparked with Ar for at least 15 min before each experiment. The linear polarization analysis was made with a potential scan from -300 to +300 mV *vs* open circuit potential (E_{ocv}) at scan rate of 0.15 mV s^{-1}. EIS was performed at E_{ocv} using a perturbation of 10 mV of amplitude, in a frequency range from 100 kHz to 5 mHz with 6 points per decade. Before each analysis, the system was allowed to reach the open circuit potential for at least 45 min.

3. Results and Discussion

3.1 Characterization of GO

The FT-IR spectrum of GO (Figure 1S) shows the band associated with the stretching vibration of the O-H bond between 3000 and 3700 cm^{-1}, mainly related to the phenolic groups and the residual water present in the sample. The bands corresponding to the stretching vibration of the double bond C=O and the O-H bending deformation of carboxylic acids appear at 1720 and 1390 cm^{-1}, respectively [28], meanwhile, the bands at 1100 and 1220 cm^{-1}, correspond to the stretching vibration of the C-O bond in alcohols and

epoxides, respectively [29]. On the other hand, the band at 600 cm^{-1} has been lately related to the ketone groups [30]. The band at 1610 cm^{-1} is associated to the skeletal vibration modes of the unaffected graphitic domains of the basal plane of the sheets [31].

Additionally, the acid groups identified in the FT-IR spectra were quantified by Boehm titrations, the results are shown in Table 1. According to these results the carboxylic and phenolic groups are present at higher proportion. However, it needs to be stated that the epoxides tend to be more reactive and undergo ring opening at basic pH. After the opening of the epoxide ring, an additional phenolic group is formed, thus, the quantity of the later is not represented correctly in these results. Since Boehm titration procedure can't correctly quantify the epoxide and phenolic groups, it can be concluded that the carboxylic groups are present in a higher proportion in GO, as it has been reported before [32].

Table 1. Concentration of acid groups in GO determined by Boehm titration.

Carboxylic (meq g^{-1})	**Lactonic** (meq g^{-1})	**Phenolic** (meq g^{-1})	**Carbonyl** (meq g^{-1})	**Total** (meq g^{-1})
1.56 ± 0.26	0.31 ± 0.08	1.75 ± 0.17	0.87 ± 0.53	4.5 ± 0.44

The presence of these acid groups at the edges and basal plane of GO grants the sheets a negative charge when suspended in water, as it can be seen by the ζ values shown in Figure 2S in the supplementary material. The curve shows a negative potential through all the pH range, exhibiting a constant value at pH values higher than 6 and reaching a value close to 0 at pH 2. As it was mentioned before, the negative potential value arises from the

deprotonation of the acid groups, such as carboxylic and phenolic groups. It has been reported that the pK_a values of carboxylic acids on graphene varies from 4 to 6 depending on its position with respect to neighboring alcohol groups, meanwhile, the pK_a value of phenolic groups is around 9 [32,33]. According to this, the behavior of ζ can be explained with the high concentration of carboxylic groups in the GO under study, with respect to the other groups. At low pH values the acid groups are protonated, hence, a value of ζ close to 0 is observed. The dissociation of acid groups increases the negative value of ζ until a pH value of 6, corresponding to the pK_a of carboxylic acids, where the more negative value of ζ is reached and, after this point, the potential value slightly decreases. Thus, the phenolic groups are not contributing in a considerable amount to the negative charge of the material, most certainly due to their low concentration in comparison to the carboxylic acids, as it was explained by the previous results.

3.1.1 Ca^{2+} adsorption onto GO

The approach used to invert the negative charge of GO was to adsorb Ca^{2+} ions onto the carbon material. Figure 1 shows the Ca^{2+} adsorption isotherms at pH 4 and 6, which were chosen as a function of the pK_a of carboxylic acids. It can be seen that the adsorption capacity q, increases about 5 times when increasing the pH from 4 to 6. One possible explanation is that electrostatic interactions between the cations and the deprotonated carboxylic acids are the main adsorption mechanism. Considering that at pH 6 the totality of carboxylic acids are negatively charged, the amount of adsorbed divalent cations exceeds the number of carboxylic groups (see Table 1) assuming a 1:2 ratio (2 deprotonated

carboxylic groups per divalent cation). Taking into account that there are only 1.56 meq of deprotonated carboxylic groups per gram of material at pH 6, the adsorbed amount of Ca^{2+} per gram would suggest a 25:1 ratio, which is not possible and, therefore, another mechanism should be responsible for most of the adsorption. There are plenty of studies about the adsorption of divalent cations on activated carbon and most of them concluded that the material acidity is the main reason for the adsorption of metals [34–36]. However, the surface area of carbon also plays an important role in the removal of metal ions, as showed by M. Valix et al. [37], the latter may be through cation-π interactions between the ions and the sp^2 domains of carbon atoms. Hence, some part of the adsorbed Ca^{2+} on GO could be via these interactions with the unoxidized graphitic domains. Additionally, it has been reported that the functional groups present in GO sheets can bond divalent metal ions and use them as cross-linkers to form agglomerates with increased mechanical and thermal properties [38,39]. The cross-linking process may lead to the formation of porous agglomerates, which results in an increase in the Ca^{2+} adsorption capacity. Also, during the agglomeration process, Ca^{2+} ions could get caught inside the agglomerate structure, thereby contributing to the high concentration of adsorbed calcium.

The approach taken in this work to invert the charge of GO was to saturate its surface with Ca^{2+} ions, which is represented by the maximum adsorption capacity of the material; however, if such high Ca^{2+} concentration is used, migration problems could occur, due to the minimizing effect that a high ionic strength has on this form of mass transport. Therefore, during the cEPD of GO, an initial Ca^{2+} concentration (C_0) of 0.1 M was used, obtaining a Ca^{2+} equilibrium concentration (C_e) of 0.08 M, which was enough to change the GO charge.

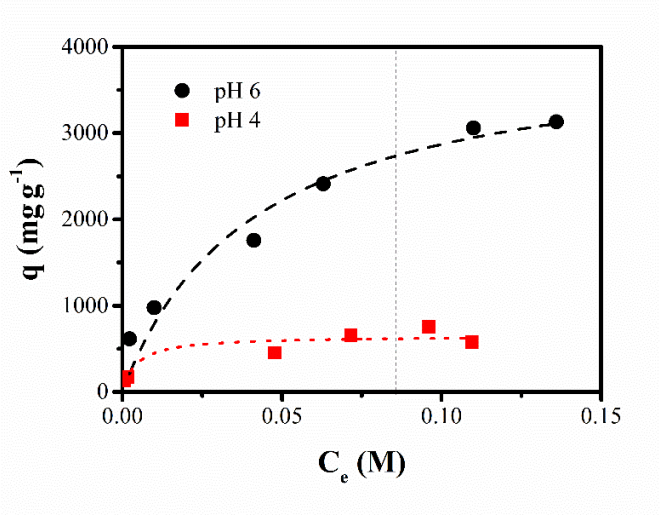

Figure 1. Ca^{2+} adsorption isotherms onto GO at pH 4 and 6, at 25 °C. Dashed line represents an equilibrium concentration of 0.08 M.

The ζ of GO shifted to positive values after the addition of Ca^{2+} ions (see Figure 2), and an increasing tendency of this value is observed as the suspension pH rises, reaching its maximum value at about 5.2 mV at pH 6. This is in agreement with Boehm titrations, since carboxylic groups are in a higher proportion in the GO and, they are mainly responsible for the Ca^{2+} adsorption. Similar results were reported by Chowdhury et al. [40], since they observed that the electrophoretic mobility of GO shifted to more positive values when a low concentration of divalent cations, such as Ca^{2+} or Mg^{2+}, were added to the suspension. The authors also observed that this effect was more noticeable when the pH of the suspension increased. However, in their work, the GO didn't reach positive values of electrophoretic mobility, probably due to the low concentration of cations used. In this work, the change of ζ`s GO sheets is attributed to the adsorption of Ca^{2+} and to the ionic strength of the suspension, which also has an effect on the double layer thickness.

According to these results, an initial Ca^{2+} concentration of 0.1 M inverts the negative ζ value of GO and enable its deposition onto the cathode during the EPD, avoiding an excess of ionic strength, which could end up in the mitigation of the mass transport by migration.

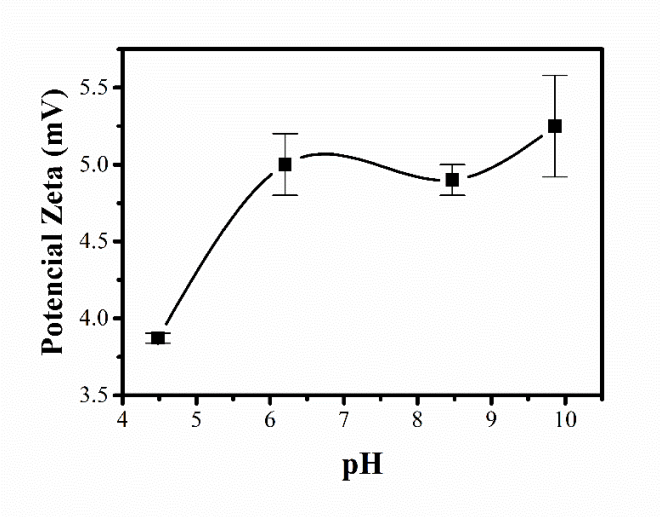

Figure 2. Zeta potential (ζ) of GO sheets suspended in an electrolytic solution with an initial Ca^{2+} concentration of 0.1 M.

3.2 Simultaneous electrochemical deposition and reduction of GO by cEPD

Once the inversion of the GO charge was achieved, the electrochemical reduction of GO was investigated using cyclic voltammetry, in order to stablish the minimum potential value to be applied during the EPD process to accomplish a simultaneous deposition and electrochemical reduction of the material. The voltammetric response of the carbon steel electrode in an electrolytic solution with an initial Ca^{2+} concentration of 0.1 M containing GO (Figure 3S) showed a cathodic peak at -1.01 V vs Ag/AgCl/NaCl (3 M), which can be attributed to the electrochemical reduction of GO, in contrast, the voltammetric response of

the same electrode in solution without GO showed no peaks. Similar responses have been reported in other works [21,31,41], even so, the electrochemical reduction mechanism of GO is not completely understood. M. Zhou et al. [21] proposed a reduction mechanism assisted by protons and proposed equation (1).

$$GO + aH^+ + be^- \rightarrow ERGO + H_2O \quad (1)$$

They observed that the voltammetric peak associated to the reduction of GO increased in intensity and appeared at more positive potentials when working at lower pH values; however, they were able to reduce the material even at pH 12, therefore indicating that the proposed mechanism may not be the only one. The authors also reported that, by electrochemical reduction of GO, they achieved a O/C ratio of 4.2 %, which they reported to be lower than the O/C achieved by chemical reduction with hydrazine, which was 6.25 % [21].

By assuring a more negative electrode potential on the cathode than the peak potential associated to the reduction of GO, during the EPD process, the simultaneous deposition and electrochemical reduction of GO will be achieved. During the cEPD of GO a cell voltage of 2.3 V was applied, which is equivalent to a cathode potential of -1.15 V vs Ag/AgCl/NaCl (3 M). According to the voltammetry response, this potential is beyond the peak potential of GO electrochemical reduction and also it is not located in the zone of water electrolysis reaction, which is well known to happen at higher potential:

$$2H_2O \rightarrow 2H_{2(g)} + O_{2(g)} \qquad \text{-1.44 V vs Ag/AgCl/NaCl (3 M)} \quad (2)$$

Additionally, no other possible parasitic reactions may occur at this potential value, such as calcium deposition:

$$Ca^{2+}_{(aq)} + 2e^{-} \rightarrow Ca_{(s)} \qquad \text{-3.08 V vs Ag/AgCl/NaCl (3 M)} \qquad (3)$$

According to the ζ values, the electrophoretic mobility of GO when suspended in the electrolytic solution of $CaCl_2$ is about 10 times lower than in water. For this reason, the voltage was applied for 90 min.

3.3 rGO film characterization

The resulting film was characterized by Raman spectroscopy, and the obtained spectra are shown in Figure 3. The presence of the rGO film on carbon steel is verified by the presence of the G and D bands in the Raman spectrum of the coated sample, which are not present in the spectrum of a clean carbon steel substrate. These bands are characteristic of carbonaceous materials, the G band, appearing at 1595 cm^{-1}, corresponds to the E_{2g} modes associated to the defect-free graphitic domains. On the other hand, the D band, appearing at 1350 cm^{-1}, is associated to the presence of unorganized carbon and a decrease in graphite crystal size [42], which has been related to the presence of vacancies and oxygenated groups introduced during the synthesis method [43]. The I_D/I_G ratio denotes the defectiveness of the sample. An increase in this ratio has been used to identify the reduction of GO to a structure with less functional groups corresponding to rGO [30,31,44,45] . The I_D/I_G of the GO sample and the carbon steel coated with GO by cEPD were 1.09 and 1.71, respectively, indicating that the reduction of GO occurred: this promoted the presence of a higher number of defects in the rGO film, showing that the sp^2 hybridization is not totally restored after the reduction process. However, according to S. Stankovich et al. [45], the sp^2

hybridization is in fact restored to some degree and the increase in the I_D/I_G ratio after the reduction process should be interpreted as an increase in the number of sp^2 domains of smaller size. Another indicator of the reduction of GO simultaneously to its deposition was an increase in the contact angle in comparison to a GO-coated carbon steel (coated by drop coating), the contact angle measurements were 58.89 ± 0.2 and 61.43 ± 1.3 for the GO-coated and rGO-coated, respectively.

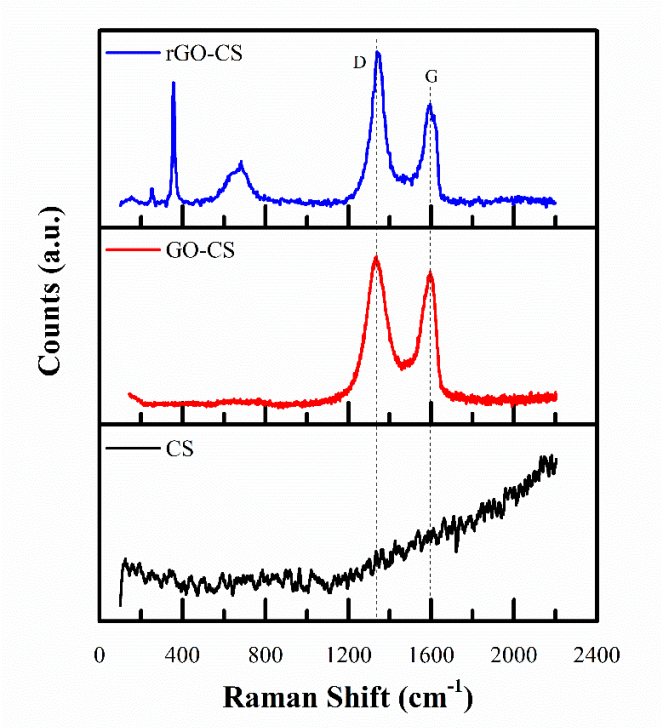

Figure 3. Raman spectra of Carbon steel, Carbon steel + GO (produced by drop coating) and Carbon steel + rGO produced by cEPD.

Additionally, the Raman spectrum of the carbon steel coated with rGO showed additional bands at 255, 355 and 685 cm^{-1}. These bands had been identified in the Raman spectra of the different crystalline forms of calcium based minerals ($CaCO_3$) such as calcite, aragonite and vaterite [46]. Additionally, some authors [47,48] have found the same peaks mentioned before in the Raman spectra of $Ca(OH)_2$, which are attributed to the two translational and one rotation modes of the OH^- against the cations [48]. According to this, the presence of these bands in the Raman spectra of carbon steel coated with the rGO film may be attributed to the Ca-O complex present in the GO agglomerates, due to the fact that the interaction cation-carboxylic acid may present the same vibrational modes than the Ca-O bond present in all the calcium minerals mentioned before.

The presence of the rGO film on the carbon steel substrate was also verified by XPS measurements. Figure 4 shows the XPS survey spectra of carbon steel, GO and the rGO film synthetized by the cEPD process. The survey spectrum of carbon steel shows a clear response of the peaks associated to Fe bonds: the peaks $Fe2p_{3/2}$ and $Fe2p_{1/2}$ located at ~710 and ~724 eV, respectively, the Fe2s at ~842 eV, the peaks Fe3p and Fe3s at ~54 and ~91 eV respectively, and the peaks Fe LMM, Fe LMM1, Fe LMM2 at ~782, ~842, ~891 eV, accordingly. Additionally, the O1s peak, related to the presence of Fe_2O_3 and FeO, appears at ~531 eV. On the other hand, the survey spectrum of the GO sample, synthetized over a carbon steel substrate by dip coating, showed only two intense peaks related to the C1s and O1s at ~285 and ~531 eV, respectively; these peaks are related to the carbon atoms in GO and its oxygenated functionalities. Moreover, the peaks related to the Fe of carbon steel are not distinguishable. On the other hand, the survey spectra of the rGO film synthetized by cEPD on the carbon steel surface showed the same peaks associated to the C1s, O1s. Also,

the spectra showed a peak at 346-350 eV related to the $Ca2p_{3/2}$ and $Ca2p_{1/2}$, which is related to Ca^{2+} bonded to oxygen, owed to the interaction of the cations with the carboxylic acids of GO. Additionally, the spectra of the rGO coated steel showed the features related to the Fe bonds in the range from 700 to 900 eV. The latter indicates that the thickness of the rGO coating is less than 10 nm. It is important to mention that the rGO coating is barely perceptible to the naked eye and it does not affect the original finish of the carbon steel substrate.

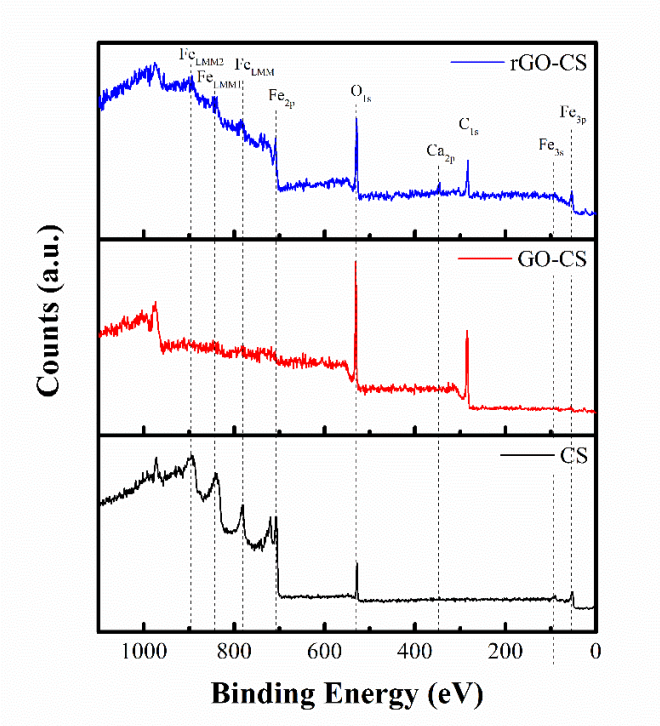

Figure 4. XPS survey spectra of carbon steel, carbon steel + GO (synthetized by drop casting) and carbon steel + rGO synthetized by cEPD.

The electrochemical reduction of GO during the cEPD was also confirmed by XPS. Figure 5 shows the high resolution XPS spectra of the C1s region of both GO and the rGO film

obtained after the cEPD process. Both spectra showed two peaks that can be deconvoluted in order to identify the chemical structures present in the material. The peaks at 244.8 and 285.6 eV represent the C=C and C-C bonded carbon related to the sp^2 and sp^3 domains in the material, respectively [49]. Meanwhile, the peaks at ~286.6, ~288.02 and ~289.5 eV represent different bonds between carbon and oxygen atoms, C-O, C=O and O-C=O, accordingly. The presence of these bonds is associated to the different oxygenated functional groups on GO. For example, the C-O bond is related to the presence of phenolic, epoxides, and carboxylic groups. The C=O bond is related to the presence of carbonyl and carboxylic groups, meanwhile, the O-C=O bond is attributed only to the latter [12,50]. Direct comparison of the spectra showed a difference in the area of the peak related to the different forms of oxygen-bonded carbon, which clearly states a decrease in their concentration after the cEPD process due to the simultaneous electrochemical reduction of the material. The latter is reflected on the increase in C/O ratio of the sample, being 0.76 and 1.4 for the GO and rGO respectively (see Table 2). The spectra in Figure 5 are direct proof of the different mechanism for the removal of the oxygenated groups in GO by an electrochemical reduction, which becomes clear when comparing these spectra to those obtained after an electrochemical oxidation process (aEPD) of GO reported by several authors. For example, according to S. An et al. [15], after the anodic EPD of GO, the carboxylic groups were mainly removed, and after the process, a small amount of phenolic groups and pretty much all the carbonyl groups were still remaining. Similar results were reported by M. Diba et al. [16], since they observed a decrease of the peak area related to carboxylic groups as function of the imposed voltage during an anodic EPD process. However, according to our results, after the electrochemical reduction of GO (cEPD), the

C-O peak showed the greatest decrease, meanwhile the peaks related to the C=O and O-C=O groups seem to be shortly affected. The latter indicates that the phenolic and epoxide were the groups mainly affected by the electrochemical reduction process, and it was more difficult to remove the carbonyl and carboxylic groups (Table 2). There are two possible explanations to these effects, the first one is that due to the complexation of the carboxylic groups with the Ca^{2+}, they became harder to be reduced electrochemically [51]. The second one is based on the reduction mechanism proposed by M. Zhou et al. [21]. According to Eq. 1, proposed by those authors, the electrochemical reduction process of GO may consist in hydrogenolysis reactions and, due to the structure of the carboxylic groups, it will take more steps for them to be completely removed in the form of H_2O with a hydrogenolysis reaction. C. Kvarnström et al. [41,52] also studied the electrochemical reduction of GO in aqueous media, they reported the importance of H^+ and intercalated water in the mechanism of reduction, which affect mainly the epoxide groups, being the carboxylic and phenolic groups harder to remove. Additionally, Figure 5 showed that the peak associated to the sp^3 bonded carbon (C-C) increased after the electrochemical reduction process, which was consistent with the Raman spectrum, meaning that after the reduction process the sp^2 hybridization was only in part restored (Table 2). The latter might be due to the electrochemical reduction mechanism of GO, consisting mainly in hydrogenolysis reactions; nevertheless, it is well known that these reactions tend to compete with hydrogenation reactions, as it is shown in Figure 6. The hydrogenation reaction of GO would end in the loss of certain degree of sp^2 hybridization and the removal of a certain concentration of oxygenated groups. This effect is reflected at the percentage of sp^3 bonded carbon from the total C-C bonds ($\frac{(C-C)}{(C=C)+(C-C)}x100$), without considering the carbon

bonded to oxygen atoms, in order to represent the hydrogenation of the graphitic domains (Table 2). The percentage of sp^3 bonded carbon increased from 40.67 to 51.84 % after the cEPD process, due to the electrochemical reduction of GO, which appears to consist in hydrogenolysis and hydrogenation reactions. This reduction mechanism is in concordance with what was observed in the Raman spectrum (Figure 3), where, there was a simultaneous removal of oxygenated groups and a certain degree of hydrogenation of the conjugated graphitic network of GO, ending up in rGO with a higher number of defects.

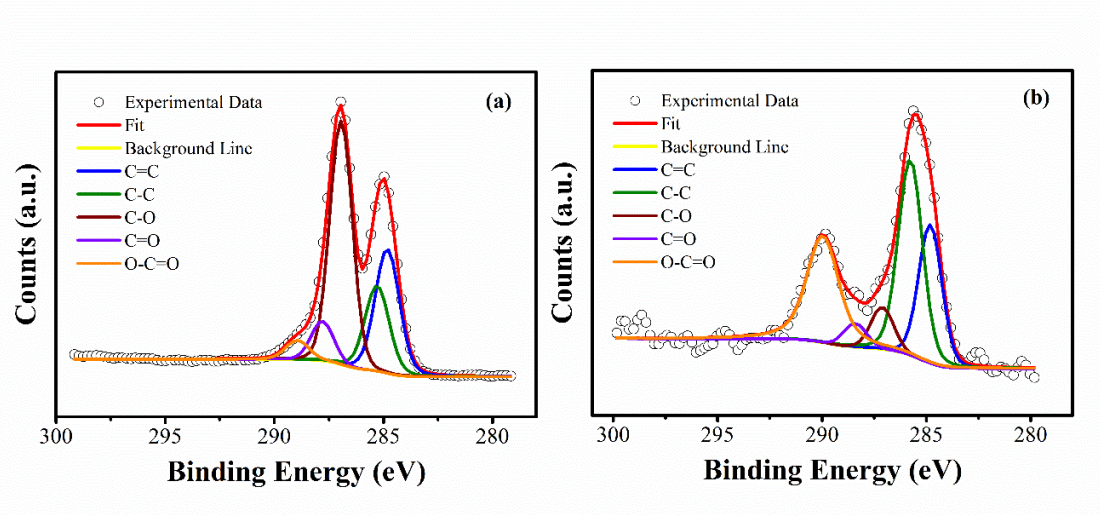

Figure 5. High resolution XPS spectra of C1s of GO (a) and rGO film (b).

Table 2. Parameters obtained from the High resolution XPS spectra of C1s of the GO and rGO films.

Sample	% C=C (284.8 eV)	% C-C (285.6 eV)	% C-O (~286.6 eV)	% C=O (~288.02 eV)	% O-C=O (~289.9 eV)	C/O	$\frac{(C-C)}{(C=C)+(C-C)}x100$ (sp^3)
GO	25.73	17.66	45.43	7.32	3.79	0.76	40.67
rGO	30.27	32.61	11.22	4.06	21.83	1.40	51.84

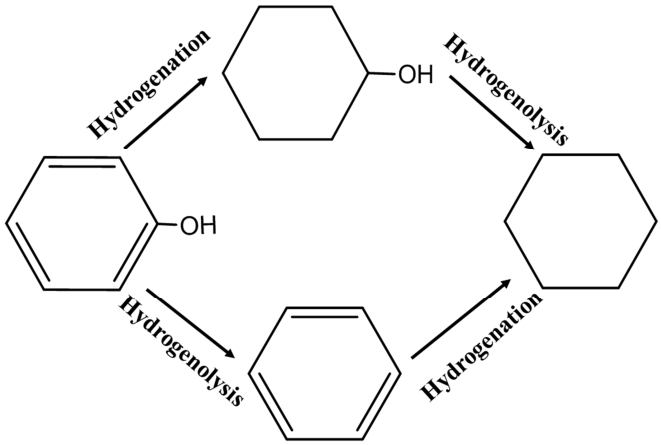

Figure 6. Possible removal mechanism of the oxygenated groups of GO via electrochemical reduction

The SEM micrographs of the carbon steel surface before (left side) and after (right side) the cEPD process are shown in Figure 7. The surface of carbon steel showed the usual topography related to a polishing with no mirror finish, where fissures and line marks were to be expected. On the other hand, the surface of the carbon steel after the cEPD had a rather different topography, presenting a rug-alike surface, which was also different from the usual smooth surface obtained after anodic EPD of GO [15,20,25,53,54]. The latter may be due to the agglomerates formed during Ca^{2+} adsorption. The irregular shape of these agglomerates could cause an uneven stacking during the formation of the deposit and, therefore, giving place to the formation of this particular topography. Nevertheless, the scanning electron micrograph shown in Figure 7b demonstrated that the rGO film adapted to the topography of the carbon steel substrate. EDS was performed on both, rGO-coated and uncoated steel samples, and the atomic % of C found was 27.36 and 19.96,

respectively. Also, there were notable differences on the atomic % of O, reaching 19.41 and 28.53 % for the coated and uncoated sample respectively. The latter may owe to corrosion presented at the uncoated sample, as this kind of steel is easily corroded under atmospheric conditions.

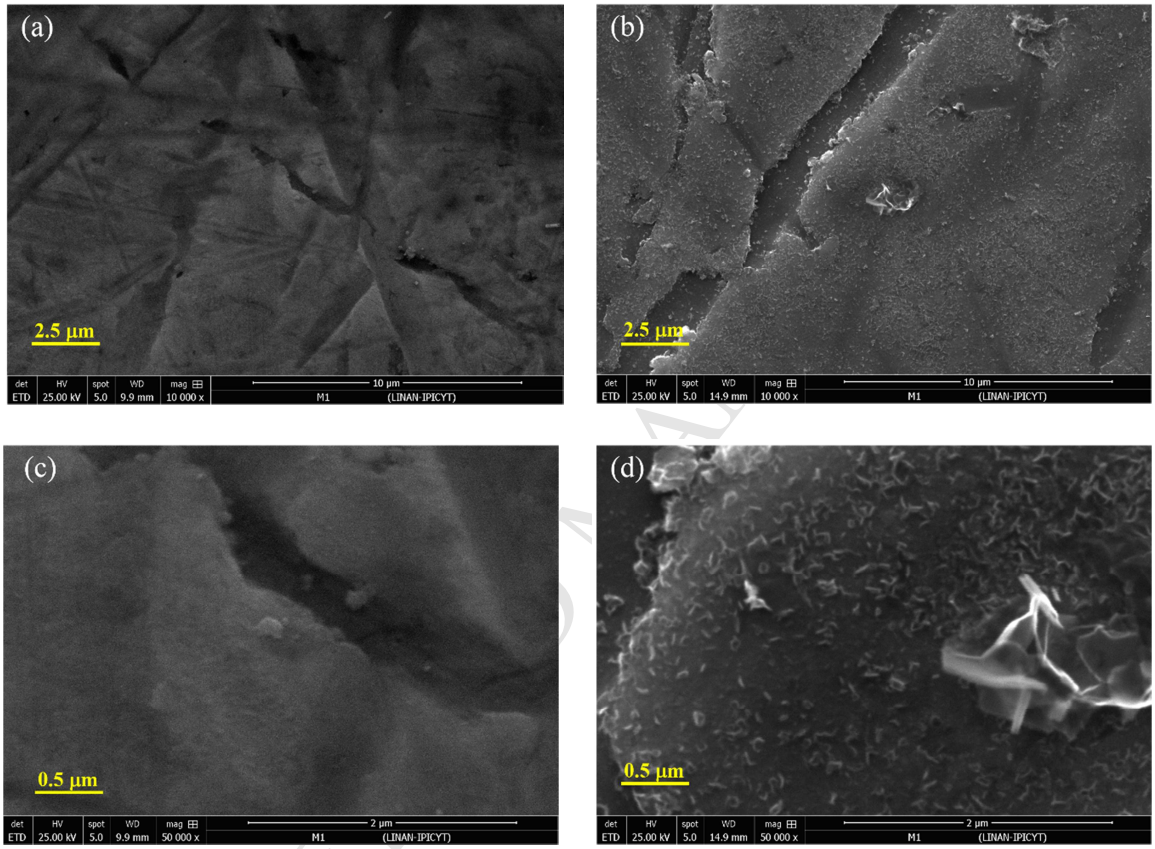

Figure 7. Micrographs of the uncoated carbon steel at low (a) and high (c) magnification, and rGO-coated carbon steel at low (b) and high (d) magnification.

3.4 Evaluation of the corrosion protection of carbon steel granted by the rGO film

The corrosion protection of the rGO film was evaluated by electrochemical techniques. Figure 8 shows the Tafel plot of the linear polarization curves of uncoated carbon steel and

rGO coated carbon steel, obtained in the corrosive medium of NaCl 3.5 %. It can be seen that the polarization curve of rGO coated carbon steel was shifted to more positive potentials; where the uncoated sample showed a corrosion potential (E_{cor}) of -0.72 ± 0.28 V, meanwhile, the coated sample showed a potential of -0.61 ± 0.13 V. This behavior is characteristic of the protection of a metal with a noble material [55], and indicates that higher potentials are needed to promote the dissolution of the metal [56]. Additionally, according to Figure 8, the polarization curve of rGO-coated carbon steel reached lower values of current. The corrosion current density, i_{cor}, was obtained by extrapolation of the kinetic behavior at high overpotentials [55], obtaining an i_{cor} of 11.83 ± 0.86 and 4.14 ± 0.64 mA cm^{-2} for the uncoated and rGO-coated carbon steel respectively. According to these results, the rGO coating synthetized by cEPD reduced by three times the corrosion rate of the carbon steel sample.

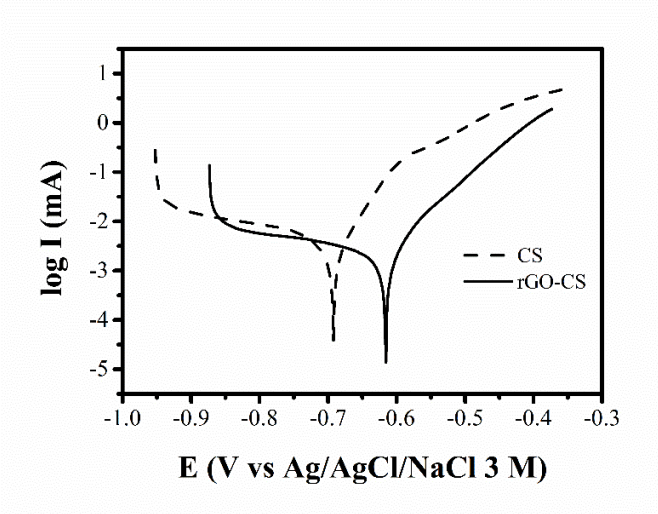

Figure 8. Tafel plot of the polarization curves of carbon steel (CS) and rGO-coated carbon steel (rGO-CS) obtained in an electrolytic solution at 3.5 % of NaCl.

Similar results have been seen before when metals, such as copper or nickel, are coated by either CVD grown graphene [6–9] or EPD rGO [18,19,22–25,53,56]. However, according to J. H. Park and J. M. Park, a rGO-coating produced by anodic EPD did not decrease the corrosion rate of a carbon steel sample [20]. These authors reported a shifting of E_{cor} to more negative potentials and no significant change in the i_{cor} of the sample after coating it with a rGO film produced by anodic electrophoretic deposition. They attributed this result to a low density deposit and to the presence of defects in the rGO film [20]. As it was mentioned before, the anodic oxidation process of GO after reaching the anode in aEPD, causes the removal of oxygenated groups, carboxylic acids specifically, by a Kolbe-like reaction [15,16], according to equations (4), (5) and (6).

$$RCOO^- \rightarrow RCOO^{\cdot} + e^- \quad (4)$$

$$RCOO^{\cdot} \rightarrow R^{\cdot} + \cdot CO_2 \quad (5)$$

$$2R^{\cdot} \rightarrow R - R \quad (6)$$

It is well accepted that this reaction mechanism promotes the formation of defects, such as vacancies, in the graphene sheets and, as it has been reported, these defects are the main reason for graphene failure as an anticorrosive coating, due to the formation of a galvanic pair and the occurrence of galvanic corrosion [26]. Also, these type of defects may be the reason of the unsuccessful application of a rGO film in the protection of carbon steel, since, unlike cooper, the oxide film formed on the unprotected carbon steel sites by the rGO film (site where the rGO defects are located) neither stops the corrosion process or passivates the sample [55]. For the case of the rGO-coating obtained by cEPD, the suggested electrochemical reduction mechanism consisting of hydrogenolysis/hydrogenation reactions may explain the successful results, since this mechanism suggest the formation of a rGO

film with defects that would actually be beneficial for its use as an anticorrosive coating, since the resulting film would have low conductivity, hydrophobic nature and no vacancies, which are key factor to avoid the occurrence of galvanic corrosion.

Even though definitive proof of the suggested mechanism is still needed, some indirect proofs had been reported before by other authors. S. A. Hasan et al. [57], achieved a cEPD of GO by lowering the pH of the suspension, they also observed a higher hydrophobicity in the film obtained by cEPD compared to one produced by aEPD, which could be attributed to the hydrogenation of the material. Also, according to J. H. Park and J. M. Park [20], after the aEPD process there was a $\Delta {}^{I_D}/_{I_G}$, before and after the reduction process, of 0.37, meanwhile, the $\Delta {}^{I_D}/_{I_G}$ in the present work was 0.62. This indicates that there are higher number of defects in the rGO film synthetized by cEPD reported in this work in comparison to the one reported by those authors. Also, the graphite crystal size, L_a, was calculated using the equation proposed by L. G. Cançado et al. [58] and the Raman data shown in Figure 3, giving a L_a value of 17.63 and 11.24 nm for the GO and rGO-coating respectively. The experimental data reported by J. H. Park et al., was also used in the same equation, giving L_a values of 22.88 and 19.03 nm for their GO and rGO-coating, respectively. According to these results, the rGO film, synthetized by cEPD, reported in this work had more defects in comparison to the film produced by aEPD reported by J. H. Park et al. However, the defects introduced to the rGO-film during a cEPD, might be different to those originated during an anodic EPD of GO, since the rGO-film assembled by cEPD decreased the i_{cor} value of the coated steel by three times in comparison to an uncoated sample.

Figure 9 shows the Nyquist plot (9a) and Phase diagrams (9b) obtained by EIS. The Nyquist plot of the rGO-coated carbon steel showed two semicircles, the first one is shown in the inset of Figure 9a and is related to the interface produced between the rGO film and the electrolytic solution. Due to the small thickness of the rGO film, the semicircle in the Nyquist Plot and the phase constant in Figure 9b are barely perceptible. On the other hand, the second semicircle attributed to the interface steel/electrolyte quickly evolved into a larger one in the Nyquist plot, which allowed seeing a third time constant in the phase diagram. This interface is caused by the formation of corrosion products on the surface of the steel and inside the rGO film, meaning that the film had a tortuous path between the rGO agglomerates, since as mentioned before cannot be considered as completely hydrophobic, allowing the diffusion of electrolyte to the steel surface. The resistance of this path in the rGO film is also shown in Figure 9a as the beginning of the characteristic response associated to finite diffusion; however, the range of frequencies was not low enough to observe a complete effect of this diffusion (due to this, it was not considered for the fitting of the experimental data). Even though it is not the objective of this work, it is relevant to point out that the thickness of the rGO coating is an important parameter that can be considered to evaluate the anticorrosive protection of a substrate, since a thicker film would present an increased difficulty for the electrolyte to reach the steel surface, thus, there is a linear relationship between coating thickness and protection granted [10]. On the other hand, the Nyquist plot of the uncoated carbon steel showed only one noticeable semicircle and an inductive behavior at low frequencies. The presence of this inductor has been related to a rearrangement of the double layer caused by the formation of corrosion products on the steel surface and their subsequent combination with the solution at the interface [59]. According to this, the phase diagram of the uncoated carbon steel is most

certainly formed by two time constants, one associated to the steel/electrolyte interface and the other one, which is almost unnoticeable in Figure 9b, to the interface formed by the adsorbed corrosion products before they mix with the solution [59]. Due to the latter, the equivalent circuit used for the fitting of the experimental data of the uncoated carbon steel consisted in two sets of a constant phase element (CPE) connected in parallel with a resistance (R), the first one, showed at low frequencies is related to the steel/electrolyte interface (CPE_{dl} and R_{CT}), while the second one, at low frequencies, corresponds to the interface produced by the adsorbed corrosion products (CPE_{ads} and R_{ads}). On the other hand, the equivalent circuit of the rGO-coated sample had an additional set of CPE and a Resistor in parallel, showed at high frequencies, attributed to the presence of the rGO film (CPE_{rGO} and R_{rGO}). The results of the fitting showed that the resistance of the rGO film is quite low, 0.7 Ω, probably due to the small thickness of the sample, which should be inferior to 10 nm. Moreover, the comparison of the charge transfer resistance of the uncoated and rGO-coated steel (R_{CT}) showed an increase from 84 to 406 Ω after coating the sample with rGO. The charge transfer resistance of a metal in this electrolytic media (NaCl 3.5 % w/v) is related to the occurrence of corrosion, where at lower R_{CT} depicts a faster corrosion rate of the sample. These results are in agreement with the results obtained with the linear polarization test and showed that the rGO film synthetized by cEPD is able to reduce the corrosion rate of carbon steel.

Additionally, a stability test was performed, in which a rGO-coated sample was sonicated during 5 minutes in ethanol and the EIS spectra were obtained before and after the sonication process. The results showed no change in the EIS spectra of the sample, thus, indicating a good adhesion of the film to the steel surface (Figure 4S).

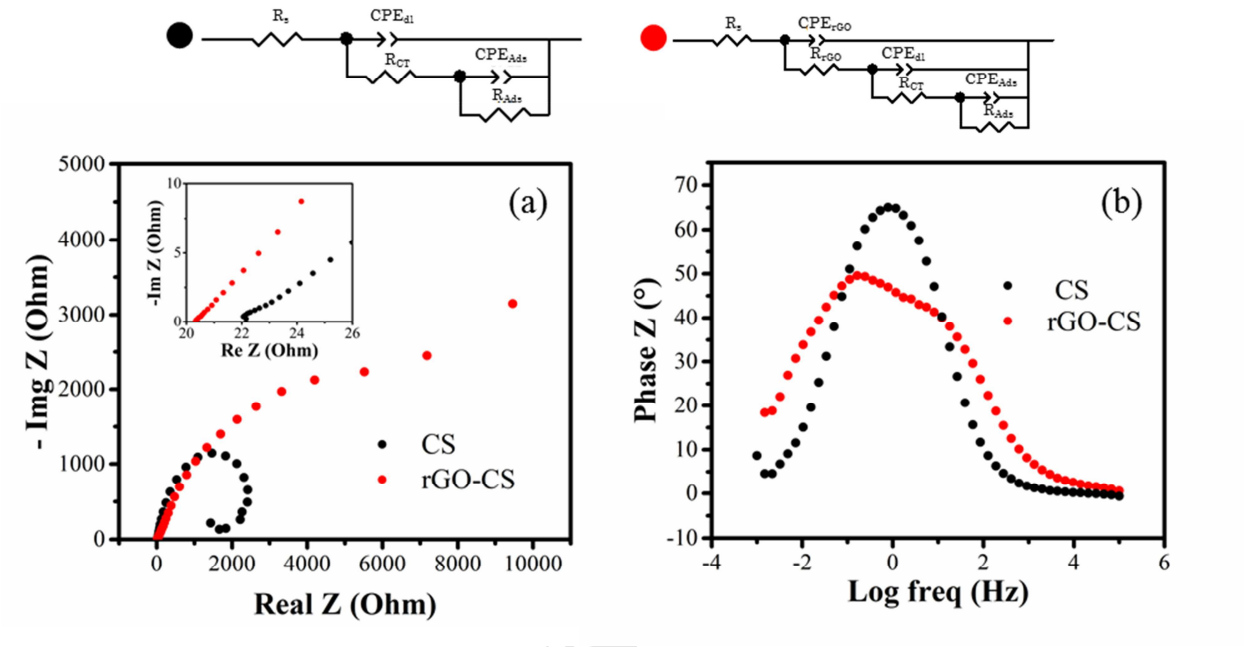

Figure 9. EIS data for carbon steel and rGO-coated carbon steel obtained in an electrolytic solution of NaCl 3.5 % w/v, Nyquist plot and (a), and phase diagrams (b).

4. Conclusions

cEPD was achieved by adding a concentration of Ca^{2+} ions to the suspension of GO. The Ca^{2+} ions interacted with the carboxylic acids and π e^- of the sp^2 domains of GO acting as cross-linkers to form positively charged agglomerates of GO. It was proposed that the electrochemical reduction mechanism of GO, which appears to consist in hydrogenation/hydrogenolysis reactions, could be an alternative via for the assemble of a rGO film that could reduce up to three times the corrosion rate of carbon steel. The later

was proved by the decrease of the I_{cor}, by a shifting of E_{cor} to more positive values, and also by an increase of the R_{CT} of carbon steel.

Acknowledgements

The authors would like to thank to CONACyT for the Ph. D. scholarship with register number: 258408 and for the financial support through the project SEP-CONACyT: 169634. Also, special thanks to Dulce Partida, Juan Pablo Rodas, Elizabeth Cortez and Guillermo Vidriales for their technical support. X-ray photoelectron spectra were obtained by Mariela Bravo-Sanchez at the National Laboratory of research in Nanoscience and Nanothecnology (LINAN). Thanks to Beatriz Rivera and Ana Iris Peña from LINAN, and María del Carmen Rocha from LANBAMA.

References

[1] A.K. Geim, K.S. Novoselov, The rise of graphene, Nat. Mater. 6 (2007) 183–191. doi:10.1038/nmat1849.

[2] C. Soldano, A. Mahmood, E. Dujardin, Production, properties and potential of graphene, Carbon N. Y. 48 (2010) 2127–2150. doi:10.1016/j.carbon.2010.01.058.

[3] F. Guo, G. Silverberg, S. Bowers, S.P. Kim, D. Datta, V. Shenoy, R.H. Hurt, Graphene-based environmental barriers, Environ. Sci. Technol. 46 (2012) 7717–7724. doi:10.1021/es301377y.

[4] J.S. Bunch, S.S. Verbridge, J.S. Alden, A.M. Van Der Zande, J.M. Parpia, H.G. Craighead, P.L. McEuen, Impermeable atomic membranes from graphene sheets,

Nano Lett. 8 (2008) 2458–2462. doi:10.1021/nl801457b.

[5] R.R. Nair, P. Blake, a N. Grigorenko, K.S. Novoselov, T.J. Booth, T. Stauber, N.M.R. Peres, a K. Geim, Fine structure constant defines visual transparency of graphene., Science. 320 (2008) 1308. doi:10.1126/science.1156965.

[6] D. Prasai, J.C. Tuberquia, R.R. Harl, G.K. Jennings, K.I. Bolotin, Graphene : Corrosion-Inhibiting Coating, ACS Nano. 6 (2012) 1102–1108. doi:10.1021/nn203507y.

[7] N.T. Kirkland, T. Schiller, N. Medhekar, N. Birbilis, Exploring graphene as a corrosion protection barrier, Corros. Sci. 56 (2012) 1–4. doi:10.1016/j.corsci.2011.12.003.

[8] R.K. Singh Raman, P. Chakraborty Banerjee, D.E. Lobo, H. Gullapalli, M. Sumandasa, A. Kumar, L. Choudhary, R. Tkacz, P.M. Ajayan, M. Majumder, Protecting copper from electrochemical degradation by graphene coating, Carbon N. Y. 50 (2012) 4040–4045. doi:10.1016/j.carbon.2012.04.048.

[9] S. Chen, L. Brown, M. Levendorf, W. Cai, S.Y. Ju, J. Edgeworth, X. Li, C.W. Magnuson, A. Velamakanni, R.D. Piner, J. Kang, J. Park, R.S. Ruoff, Oxidation resistance of graphene-coated Cu and Cu/Ni alloy, ACS Nano. 5 (2011) 1321–1327. doi:10.1021/nn103028d.

[10] A.C. Stoot, L. Camilli, S.-A. Spiegelhauer, F. Yu, P. Bøggild, Multilayer graphene for long-term corrosion protection of stainless steel bipolar plates for polymer electrolyte membrane fuel cell, J. Power Sources. 293 (2015) 846–851. doi:10.1016/j.jpowsour.2015.06.009.

[11] V. Singh, D. Joung, L. Zhai, S. Das, S.I. Khondaker, S. Seal, Graphene based materials: Past, present and future, Prog. Mater. Sci. 56 (2011) 1178–1271. doi:10.1016/j.pmatsci.2011.03.003.

[12] S. Pei, H.M. Cheng, The reduction of graphene oxide, Carbon N. Y. 50 (2012) 3210–3228. doi:10.1016/j.carbon.2011.11.010.

[13] D.R. Dreyer, S. Park, C.W. Bielawski, R.S. Ruoff, The chemistry of graphene oxide, Chem. Soc. Rev. 39 (2010) 228–240. doi:10.1039/b917103g.

[14] J.H. Dickerson, A.R. Boccaccini, Electrophoretic Deposition of Nanomaterials, Springer Science+Business Media, New York, USA, 2012. doi:10.1007/978-1-4419-9730-2.

[15] S.J. An, Y. Zhu, S.H. Lee, M.D. Stoller, T. Emilsson, S. Park, A. Velamakanni, J. An, R.S. Ruoff, Thin film fabrication and simultaneous anodic reduction of deposited graphene oxide platelets by electrophoretic deposition, J. Phys. Chem. Lett. 1 (2010) 1259–1263. doi:10.1021/jz100080c.

[16] M. Diba, A. Garcia-Gallastegui, R.N. Klupp Taylor, F. Pishbin, M.P. Ryan, M.S.P. Shaffer, A.R. Boccaccini, Quantitative evaluation of electrophoretic deposition kinetics of graphene oxide, Carbon N. Y. 67 (2014) 656–661. doi:10.1016/j.carbon.2013.10.041.

[17] a. Chavez-Valdez, M.S.P. Shaffer, a. R. Boccaccini, Applications of graphene electrophoretic deposition. A review, J. Phys. Chem. B. 117 (2013) 1502–1515. doi:10.1021/jp3064917.

[18] E.T.Y. Lih, R.B.M. Zaid, L.L. Tan, K.F. Chong, Facile Corrosion Protection Coating

from Graphene, Int. J. Chem. Eng. Appl. 3 (2012) 453–455. doi:10.7763/IJCEA.2012.V3.242.

[19] S.C. Sahu, A.K. Samantara, M. Seth, S. Parwaiz, B.P. Singh, P.C. Rath, B.K. Jena, A facile electrochemical approach for development of highly corrosion protective coatings using graphene nanosheets, Electrochem. Commun. 32 (2013) 22–26. doi:10.1016/j.elecom.2013.03.032.

[20] J.H. Park, J.M. Park, Electrophoretic deposition of graphene oxide on mild carbon steel for anti-corrosion application, Surf. Coatings Technol. 254 (2014) 167–174. doi:10.1016/j.surfcoat.2014.06.007.

[21] M. Zhou, Y. Wang, Y. Zhai, J. Zhai, W. Ren, F. Wang, S. Dong, Controlled synthesis of large-area and patterned electrochemically reduced graphene oxide films, Chem. - A Eur. J. 15 (2009) 6116–6120. doi:10.1002/chem.200900596.

[22] B.P. Singh, S. Nayak, K.K. Nanda, B.K. Jena, S. Bhattacharjee, L. Besra, The production of a corrosion resistant graphene reinforced composite coating on copper by electrophoretic deposition, Carbon N. Y. 61 (2013) 47–56. doi:10.1016/j.carbon.2013.04.063.

[23] R. Li, J. Liang, Y. Hou, Q. Chu, Enhanced corrosion performance of Zn coating by incorporating graphene oxide electrodeposited from deep eutectic solvent, RSC Adv. 5 (2015) 60698–60707. doi:10.1039/C5RA11577A.

[24] C. Liu, F. Su, J. Liang, Producing cobalt-graphene composite coating by pulse electrodeposition with excellent wear and corrosion resistance, Appl. Surf. Sci. 351 (2015) 889–896. doi:10.1016/j.apsusc.2015.06.018.

[25] H. Zhang, X. Zhang, D. Zhang, X. Sun, H. Lin, C. Wang, One-Step Electrophoretic Deposition of Reduced Graphene Oxide and Ni(OH) 2 Composite Films for Controlled Syntheses Supercapacitor Electrodes, J. Phys. Chem. B. 117 (2012) 1616–1627. doi:10.1021/jp305198j.

[26] M. Schriver, W. Regan, W. Gannett, A.M. Zaniewski, F. Michael, Graphene as a Long-term Metal Oxidation Barrier : Worse Than Nothing, ACS. 7 (2013) 5763–5768.

[27] H.P. Boehm, Some aspects of the surface chemistry of carbon blacks and other carbons, Carbon N. Y. 32 (1994) 759–769. doi:10.1016/0008-6223(94)90031-0.

[28] Y. Harima, S. Setodoi, I. Imae, K. Komaguchi, Y. Ooyama, J. Ohshita, H. Mizota, J. Yano, Electrochemical reduction of graphene oxide in organic solvents, Electrochim. Acta. 56 (2011) 5363–5368. doi:10.1016/j.electacta.2011.03.117.

[29] J. Song, X. Wang, C.-T. Chang, Preparation and Characterization of Graphene Oxide, J. Nanomater. Article ID (2014) 6. doi:10.1155/2014/276143.

[30] E. Toral-Sánchez, J.A. Ascacio Valdés, C.N. Aguilar, F.J. Cervantes, J.R. Rangel-Mendez, Role of the intrinsic properties of partially reduced graphene oxides on the chemical transformation of iopromide, Carbon N. Y. 99 (2016) 456–465. doi:10.1016/j.carbon.2015.12.067.

[31] H.-L. Guo, X.-F. Wang, Q.-Y. Qian, F.-B. Wang, X.-H. Xia, A green approach to the synthesis of graphene nanosheets., ACS Nano. 3 (2009) 2653–2659. doi:10.1021/nn900227d.

[32] E.S. Orth, J.G.L. Ferreira, J.E.S. Fonsaca, S.F. Blaskievicz, S.H. Domingues, A.

Dasgupta, M. Terrones, A.J.G. Zarbin, PKa determination of graphene-like materials: Validating chemical functionalization, J. Colloid Interface Sci. 467 (2016) 239–244. doi:10.1016/j.jcis.2016.01.013.

[33] B. Konkena, S. Vasudevan, Understanding aqueous dispersibility of graphene oxide and reduced graphene oxide through p K a measurements, J. Phys. Chem. Lett. 3 (2012) 867–872. doi:10.1021/jz300236w.

[34] R. Baccar, J. Bouzid, M. Feki, A. Montiel, Preparation of activated carbon from Tunisian olive-waste cakes and its application for adsorption of heavy metal ions, J. Hazard. Mater. 162 (2009) 1522–1529. doi:10.1016/j.jhazmat.2008.06.041.

[35] G. Li, J. Shang, Y. Wang, Y. Li, H. Gao, Effect of calcium on adsorption capacity of powdered activated carbon, J. Environ. Sci. (China). 25 (2013) S101–S105. doi:10.1016/S1001-0742(14)60636-7.

[36] M.A. Alvarez-Merino, V. Lopez-Ramon, C. Moreno-Castilla, A study of the static and dynamic adsorption of Zn(II) ions on carbon materials from aqueous solutions, J. Colloid Interface Sci. 288 (2005) 335–341. doi:10.1016/j.jcis.2005.03.025.

[37] M. Valix, W.H. Cheung, K. Zhang, Role of heteroatoms in activated carbon for removal of hexavalent chromium from wastewaters, J. Hazard. Mater. 135 (2006) 395–405. doi:10.1016/j.jhazmat.2005.11.077.

[38] S. Park, K.-S. Lee, G. Bozoklu, W. Cai, S.T. Nguyen, R.S. Ruoff, Graphene oxide papers modified by divalent ions-enhancing mechanical properties via chemical cross-linking., ACS Nano. 2 (2008) 572–578. doi:10.1021/nn700349a.

[39] W. Yu, H. Xie, F. Li, J. Zhao, Z. Zhang, Significant thermal conductivity

enhancement in graphene oxide papers modified with alkaline earth metal ions, Appl. Phys. Lett. 103 (2013) 1–5. doi:10.1063/1.4824346.

[40] I. Chowdhury, N.D. Mansukhani, L.M. Guiney, M.C. Hersam, D. Bouchard, Aggregation and Stability of Reduced Graphene Oxide: Complex Roles of Divalent Cations, pH, and Natural Organic Matter, Environ. Sci. Technol. 49 (2015) 10886–10893. doi:10.1021/acs.est.5b01866.

[41] J. Kauppila, P. Kunnas, P. Damlin, A. Viinikanoja, C. Kvarnström, Electrochemical reduction of graphene oxide films in aqueous and organic solutions, Electrochim. Acta. 89 (2013) 84–89. doi:10.1016/j.electacta.2012.10.153.

[42] F. Tuinstra, L. Koenig, Raman Spectrum of Graphite, J. Chem. Phys. 53 (1970) 1126–1130. doi:10.1063/1.1674108.

[43] S. Park, R.S. Ruoff, Chemical methods for the production of graphenes, 4 (2009) 45–47. doi:10.1038/nnano.2009.58.

[44] R. Panigrahi, S.K. Srivastava, Selective reduction of graphite oxide: a novel approach, RSC Adv. 4 (2014) 53055–53059. doi:10.1039/C4RA11341A.

[45] S. Stankovich, D.A. Dikin, R.D. Piner, K.A. Kohlhaas, A. Kleinhammes, Y. Jia, Y. Wu, S.T. Nguyen, R.S. Ruoff, Synthesis of graphene-based nanosheets via chemical reduction of exfoliated graphite oxide, Carbon N. Y. 45 (2007) 1558–1565. doi:10.1016/j.carbon.2007.02.034.

[46] U. Wehrmeister, D.E. Jacob, A.L. Soldati, N. Loges, T. Häger, W. Hofmeister, Amorphous, nanocrystalline and crystalline calcium carbonates in biological materials, J. Raman Spectrosc. 42 (2011) 926–935. doi:10.1002/jrs.2835.

[47] A. Aminzadeh, Fluorescence bands in the FT-Raman spectra of some calcium minerals, Spectrochim. Acta Part A. 53 (1997) 693–697.

[48] O. Chaix-Pkuchery, D. Ciosmak, J.C. Niepce, M. Peyrard, Raman Study of Prereactional Transformations in Calcium Hydroxide Crystals during a Thermal Treatment Leading to Dehydration, J. Solid State Chem. 53 (1984) 273–276.

[49] A. Ambrosi, M. Pumera, Precise tuning of surface composition and electron-transfer properties of graphene oxide films through electroreduction, Chem. - A Eur. J. 19 (2013) 4748–4753. doi:10.1002/chem.201204226.

[50] Z. Bo, X. Shuai, S. Mao, H. Yang, J. Qian, J. Chen, J. Yan, K. Cen, Green preparation of reduced graphene oxide for sensing and energy storage applications., Sci. Rep. 4 (2014) 4684. doi:10.1038/srep04684.

[51] N.R. Joseph, The dissociation constants of organic calcium complexes, J. Biol. Chem. 164 (1946) 529–542.

[52] A. Viinikanoja, Z. Wang, J. Kauppila, C. Kvarnström, Electrochemical reduction of graphene oxide and its in situ spectroelectrochemical characterization., Phys. Chem. Chem. Phys. 14 (2012) 14003–9. doi:10.1039/c2cp42253k.

[53] W. He, L. Zhu, H. Chen, H. Nan, W. Li, H. Liu, Y. Wang, Electrophoretic deposition of graphene oxide as a corrosion inhibitor for sintered NdFeB, Appl. Surf. Sci. 279 (2013) 416–423. doi:10.1016/j.apsusc.2013.04.130.

[54] V. Mišković-Stanković, I. Jevremović, I. Jung, K. Rhee, Electrochemical study of corrosion behavior of graphene coatings on copper and aluminum in a chloride solution, Carbon N. Y. 75 (2014) 335–344. doi:10.1016/j.carbon.2014.04.012.

[55] E. Mccafferty, Introduction to Corrosion Science, Springer Science+Business Media, New York, USA, 2010. doi:10.1007/978-1-4419-0455-3.

[56] C.M.P. Kumar, T. V. Venkatesha, R. Shabadi, Preparation and corrosion behavior of Ni and Ni-graphene composite coatings, Mater. Res. Bull. 48 (2013) 1477–1483. doi:10.1016/j.materresbull.2012.12.064.

[57] S. a Hasan, J.L. Rigueur, R.R. Harl, A.J. Krejci, I. Gonzalo-Juan, B.R. Rogers, J.H. Dickerson, SI-Transferable graphene oxide films with tunable microstructures., ACS Nano. 4 (2010) 7367–7372.

[58] L.G. Caņado, K. Takai, T. Enoki, M. Endo, Y.A. Kim, H. Mizusaki, A. Jorio, L.N. Coelho, R. Magalhães-Paniago, M.A. Pimenta, General equation for the determination of the crystallite size la of nanographite by Raman spectroscopy, Appl. Phys. Lett. 88 (2006) 191–194. doi:10.1063/1.2196057.

[59] R. Antao-Lopez, M. Keddam, H. Takenouti, A new experimental approach to the time-constants of electrochemical impedance: Frequency response of the double layer capacitance, Electrochim. Acta. 46 (2001) 3611–3617. doi:10.1016/S0013-4686(01)00640-5.

Synthesis of reduced graphene oxide (rGO) films onto carbon steel by cathodic electrophoretic deposition: anticorrosive coating

J. A. Quezada-Rentería, L. F. Cházaro-Ruiz*, J. R. Rangel-Mendez*

Highlights

- Ca^{2+} allows the electrophoretic deposition of GO onto the cathode.
- A cross-linker effect occurred between Ca^{2+} and GO's carboxylic groups.
- Electrochemical reduction of GO and its deposition was achieved simultaneously.
- The GO reduction by hydrogenolysis/hydrogenation reactions is suggested.
- The rGO film reduces up to three times the corrosion of carbon steel.